Supplementary Information

Probing Catalytic Heterogeneity of Single FeCo and FeCoNi Hydroxide Nanoneedles by Scanning Electrochemical Microscopy

A. Anto Jeffery, [a,b] *Tianyu Bo* [a,b] *Gaukhar Askarova* [a,b] *and Michael V. Mirkin* *[a,b,c]

[a.] *Department of Chemistry and Biochemistry, Queens College, Flushing, NY 11367*

[b.] *The Graduate Center of CUNY, New York, NY 10016*

[c.] *Advanced Science Research Center at The Graduate Center, CUNY, New York, NY 10031*

[d.] *Present address: Environmental Science and Engineering Laboratory, Department of Civil Engineering, Yeungnam University, Gyeongsan, 38541, Republic of Korea*

* Corresponding author.

e-mail: *mmirkin@qc.cuny.edu*

Table of Contents

Experimental

Materials. Ferrocenemethanol (Fc, 97%, Alfa Aesar) was sublimed before the experiments. All other chemicals were of analytical grade and used without further purification. Iron nitrate nonahydrate (99.99%), cobalt nitrate hexahydrate (99.99%), nickel nitrate hexahydrate (99.99%), ammonium fluoride (99.99%), and anhydrous absolute ethanol (99.5%) were from Sigma Aldrich. A borate buffer (BB) solution (pH 8.5) was prepared using anhydrous boric acid (99.5%) from Alfa Aesar, sodium hydroxide (97.0%) from Pellets and sodium sulfate from J.T. Baker Chemical Co. Aqueous solutions were prepared using deionized water from Milli-Q Advantage A10 system equipped with Q-Gard T2 Pak, a quantum TEX cartridge, and a VOC Pak. Highly oriented pyrolytic graphite (HOPG) of ZYB grade was obtained from K-Tek.

Synthesis of trimetallic FeCoNi hydroxide and bimetallic FeCo hydroxide nanoneedles. Trimetallic FeCoNi hydroxide particles were synthesized by a hydrothermal route (Scheme 1). Briefly, iron nitrate nonahydrate, cobalt nitrate hexahydrate, and nickel nitrate hexahydrate of equimolar composition were first dissolved in 80 ml of distilled water through ultrasonication. Ammonium fluoride (5 mmol) and urea (2.5 mmol) were further added to the solution, and sonication was continued until clear solution was obtained. This solution was transferred to a Teflon-lined autoclave, sealed well, and heated at 120 ºC for 16 h in an air oven. After hydrothermal reaction, the autoclave was cooled to room temperature, and precipitate was washed 5 times with distilled water and then with absolute ethanol and dried at ambient temperature. The synthesized FeCoNi hydroxide nanomaterials exhibited a 1D nanoneedle-type structure. The synthesis of bimetallic FeCo hydroxide nanoneedles was similar to that of trimetallic needles, but nickel nitrate hexahydrate was not added to the solution. For trimetallic nanoneedles, the mole ratio of Fe:Co:Ni was kept to 1:1.1:1.1, while for bimetallic nanoneedles the mole ratio of Fe:Co was 1.2:1.7.

Characterization of tri- and bimetallic nanoneedles. The crystal structures of synthesized materials were analysed

Scheme 1 Synthesis of trimetallic FeCoNi hydroxide nanoneedles.

by X-ray diffraction (XRD) patterns using D/MAX-2200 Ultima instrument (Rigaku Corporation). The morphology and microstructure of the synthesized materials was characterized by field emission scanning electron microscopy (FESEM) using Hitachi S-4800 microscope at a voltage of 10 kV. X-ray photoelectron spectroscopy (XPS) measurements were carried out using Thermoscientific K-alpha+ spectrometer with the anode Al Kα X-ray source with pass energy of 1-400 eV. All binding energies were calibrated with reference to C1s peak at 284.5 eV.

Bulk electrochemical experiments. The bulk electrochemical experiments were carried out with an Autolab PGSTAT potentiostat using a standard three-electrode setup with rotating disk electrode (RDE, 5 mm diameter), Pt wire working electrode, and Ag/AgCl reference, and a Pt counter electrode. The catalyst ink was prepared by dispersing either tri- or bimetallic needles (5 mg) in a mixture of 2-propanol (250 µL) and ethanol (250 µL) through ultrasonication for 5 minutes. A drop of catalyst ink was applied to the RDE and then dried at room temperature to give a mass loading of ~0.25 mg/cm^2. Linear sweep voltammograms (LSVs) were obtained with a scan rate of 5 mV/s in N_2-saturated 0.1 M KOH. Chronoamperograms were recorded in 0.1 M KOH under N_2 atmosphere for a duration of 24 hrs under at a desired potential and 1600 rpm. Electrochemical impedance spectroscopy (EIS) was performed with the frequency range 0.01 Hz to 10^5 Hz and 5 mV AC amplitude at the DC potential of 1.6 V.

SECM substrate preparation. To prepare the sample for SECM measurements, either tri- or bimetallic needles (~5 mg) were dispersed in absolute ethanol for 5 minutes to form a colloidal dispersion. 5 µL of the colloidal dispersion was applied to the HOPG substrate by spin coating and dried at 60º C for about an hour in air oven. After drying, specific needles attached to HOPG were selected, labelled using an optical microscope, and further characterized by SECM and SEM-EDS.

Fabrication and characterization of SECM Tips. Platinum nanoelectrodes were prepared by pulling and heat sealing 25 µm diameter Pt wires (Goodfellow) into borosilicate glass capillaries (Drummond; OD – 1.0 mm; ID – 0.2 mm) under vacuum with a P-2000 laser pipet puller from Sutter Instrument Co., polished on a 50 nm alumina pad

(Precision Surfaces International) under video microscopic control as reported previously[1] and sonicated in deionized water for 1 min. The appropriate protection was used to avoid electrostatic damage to the nanotips.[2] The nanoelectrodes were characterized by steady-state voltammetry, and SECM approach curves in a 1 mM FcMeOH redox mediator.

SECM setup and procedures. SECM experiments were carried out using a home-built instrument similar to that described previously.[3] The four-electrode setup was used with an Ag/AgCl reference electrode (CH Instruments) and a 1 mm Pt wire as a counter electrode. All experiments were carried out in a Faraday cage at room temperature (23 ± 2 °C). The current offset of the potentiostat (~2.5 pA) was subtracted from all measured current values. The 0.1M borate buffer was prepared by dissolving 0.6214 g of anhydrous boric acid and 0.1031 g of sodium hydroxide in 100 mL of deionized water.

The tip was brought within ~20 µm vertical distance above the HOPG surface using a manual micromanipulator and a stereo microscope. A current *vs.* distance curve was obtained using the piezo controlled z-stage during the subsequent fine approach. The tip was then moved laterally (in the x-y plane) at a constant separation distance of 1–2 tip radii from the substrate surface to locate and cross scan the needles. The negative feedback mode of SECM (Figure 1a) was used to locate a needle and establish the zero tip–substrate separation point. SECM experiments were performed in a 0.1 M BB (pH 8.5) that contained 0.5 M Na_2SO_4 as electrolyte and no added redox species except dissolved O_2. In the negative feedback mode of SECM, the Pt tip was biased at -0.6 V for ORR to occur on its surface. The mapping of water oxidation activity on the nanoneedle surface was done in the SG/TC mode (Figure 1B) with the substrate potential, E_S = 0.5 V suitable for OER. No oxygen bubble formation was detected in SECM experiments at the selected potentials and under given conditions.

AFM characterization of nanoneedles. An XE-120 scanning probe microscope (Park Systems) was used for AFM imaging of the samples. Topography imaging was carried out in a noncontact mode using PPP-NCHR ADM probes (Nanosensors).

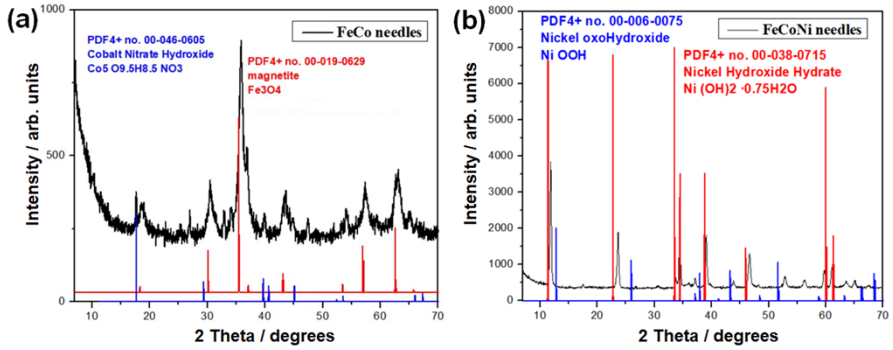

Figure S1. PXRD patterns matched with suitable phase using ICDD, PDF 4+ database for (a) FeCo nanoneedles, (b) FeCoNi nanoneedles.

The basal reflection at around 10º (2θ) clearly indicates the formation of LDH with hydrotalcite-like structure for trimetallic FeCoNi nanoneedles (Figure S1b).[4,5] However, for bimetallic FeCo nanoneedles under identical experimental conditions, the reflection was rather very weak or partially formed structure resembling more like brucite-type hydroxides and/or magnetite-type phase (PDF 4+ No. 00-019-0629, Figure S1a).[6] The reflections for FeCoNi nanoneedles (Figure S1b) corresponding to the lattice planes of (003), (006), (012), (009), (018), (110), and (113) at 2θ values 11.89º, 23.61º, 34.40º, 38.96º, 46.63º, 59.65º, and 60.95º correspond to $Ni(OH)_2$-type structure (PDF 4+ No. 00-038-0715) in which $Ni(OH)_2$ act as the host and the introduction of Fe and Co decrease the lattice parameter (Figure S1). These reflections match well with previously reported values. [4,5]

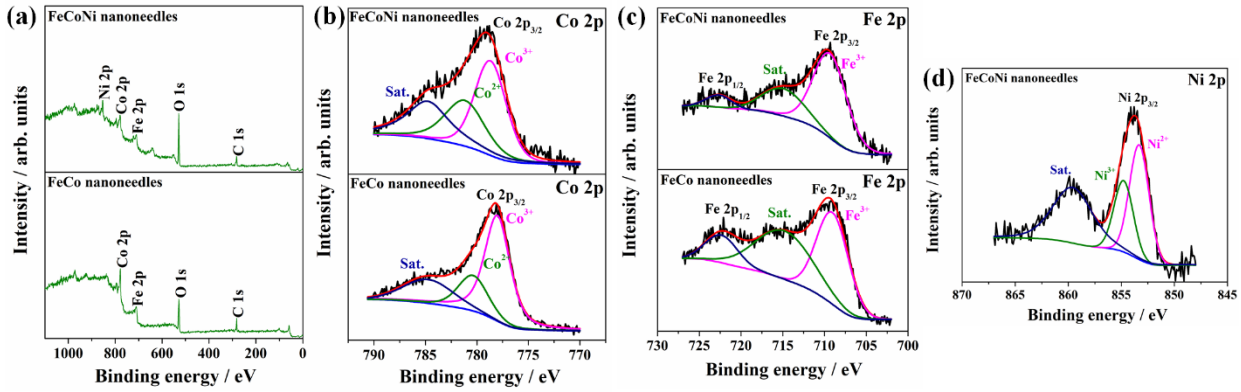

Figure S2. (a) XPS wide-scan survey spectra of trimetallic FeCoNi hydroxide nanoneedles and bimetallic FeCo hydroxide needles (b) Co 2p core-level spectra of trimetallic FeCoNi hydroxide and bimetallic FeCo hydroxide nanoneedles. (c) Fe 2p core-level spectra of trimetallic FeCoNi hydroxide and bimetallic FeCo hydroxide nanoneedles (d) Ni 2p core-level spectra of trimetallic FeCoNi hydroxide nanoneedles.

For trimetallic nanoneedles, the high-resolution spectra of the core-level regions of Co $2p_{3/2}$, Ni $2p_{3/2}$ and Fe $2p_{3/2}$ states (Figures S2b, S2c, and S2d) show the existence of multi-valent states of Co^{2+}/Co^{3+}, Ni^{2+}/Ni^{3+} and Fe^{3+}, while bimetallic nanoneedles comprise Co^{2+}/Co^{3+} and Fe^{3+} states in their core-level regions, possibly due to surface oxidation, further indicating the formation of brucite-like hydroxide structure.[6] The addition of the third metal (nickel) into FeCo hydroxide layers has caused the coexistence of Ni^{2+}/Ni^{3+} in Ni $2p_{3/2}$ state at binding energies of 853.3 eV and 854.8 eV, respectively (Figure S2d). For trimetallic nanoneedle, the two peaks at 778.7 and 781.2 eV correspond to binding energies of Co^{3+} and Co^{2+} (Figure S2b), showing a clear upward shift toward higher binding energy in comparison to bimetallic nanoneedles (Co^{3+} at 778.1 eV and Co^{2+} at 780.4 eV). This positive shift of the peaks is explicitly seen in Fe 2p spectra (Figure S2c), strongly suggesting the formation of LDH-structure of trimetallic FeCoNi hydroxide nanoneedles.[7,8,9] The peak shift to high-binding energy could also be attributed to the multi-component nature of trimetallic species that significantly modulates the electronic structure of LDH layer and enhanced charge-transfer among multi-metals, which is expected to enhance the conductivity and overall electrocatalytic performance by optimizing the adsorption/desorption energy of reactive intermediates.[10,11,12]

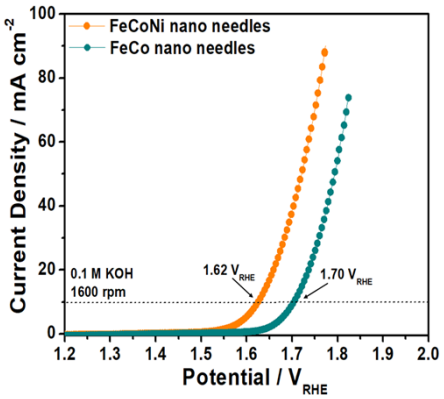

Figure S3. LSVs of OER at trimetallic (FeCoNi; orange symbols) and bimetallic (FeCo; green symbols) nanoneedles measured at 1600 rpm in 0.1 M KOH.

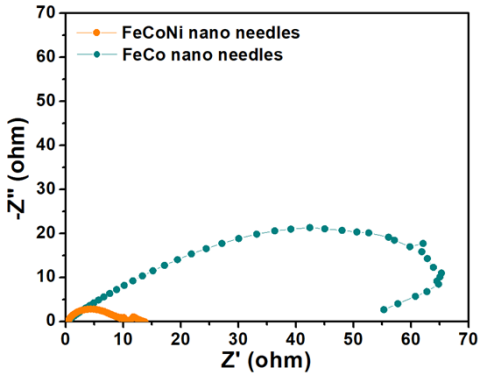

Figure S4. EIS spectra of trimetallic (FeCoNi) and bimetallic (FeCo) nanoneedles measured at the potential of 1.6 V vs RHE under 1600 rpm in 0.1 M KOH.

Figure S5. 24-hour-long current – time recordings for OER at (a) bimetallic (FeCo) and trimetallic (FeCoNi) nanoneedles measured at the potential (a) 1.7 V and (b) 1.62 V under 1600 rpm in 0.1 M KOH.

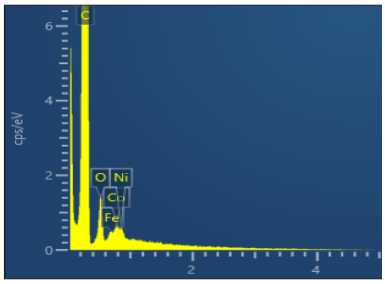

Figure S6. EDS spectra depicting the presence of Fe, Co, Ni, and O in the trimetallic needle imaged in Figure 2.

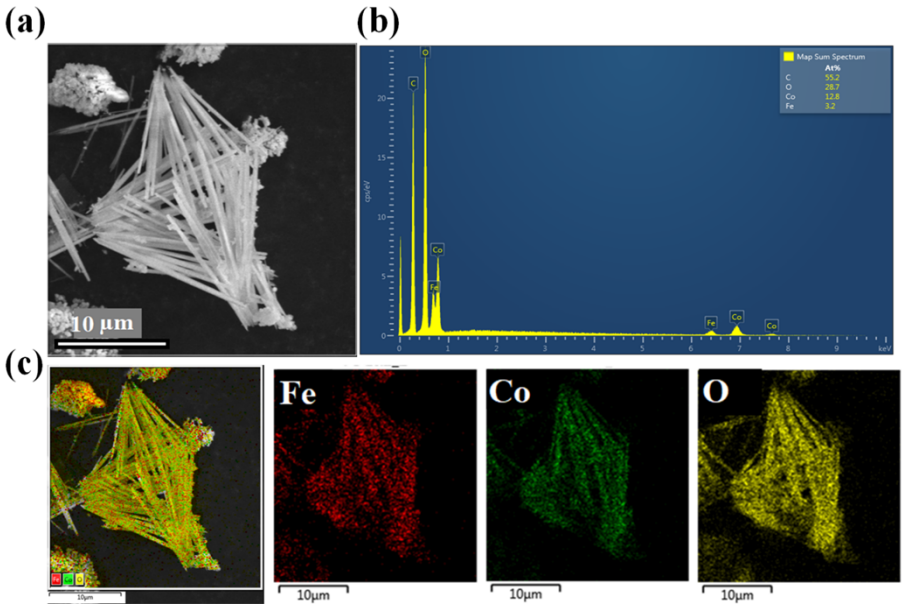

Figure S7. (a) HRSEM images of bimetallic bulk FeCo nanoneedle clusters (b) elemental spectra depicting the presence of Fe, Co, and O with their atomic percentages (c) elemental mapping of the corresponding Fe, Co, and O showing homogenous distribution of elements.

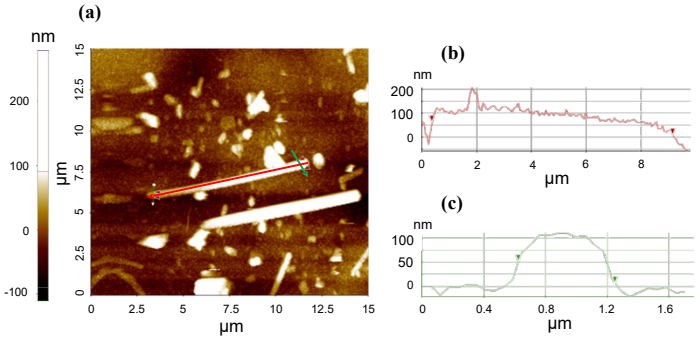

Figure S8. (a) Non-contact mode topographic AFM images of the target FeCoNiOH nanoneedle and cross sections along (b) the length and (c) the width of needle.

References

1 P. Sun and M. V. Mirkin, *Anal. Chem.*, 2006, **78**, 6526–6534.
2 N. Nioradze, R. Chen, J. Kim, M. Shen, P. Santhosh and S. Amemiya, *Anal. Chem.*, 2013, **85**, 6198–6202.
3 T. Bo, X. Wang, R. Jia, L. Han, H. L. Xin, H. Zhang, E. M. Miller and M. V. Mirkin, *J. Phys. Chem. C*, 2021, **125**, 25525–25532.
4 F. Li, Z. Sun, H. Jiang, Z. Ma, Q. Wang and F. Qu, *Energy Fuels*, 2020, **34**, 11628–11636.
5 J. Zhang, L. Jin, P. Gu, L. Hu, D. Chen, J. He, Q. Xu and J. Lu, *ACS Appl. Nano Mater.*, 2021, **4**, 12407–12414.
6 R. Ma, Z. Liu, K. Takada, N. Iyi, Y. Bando and T. Sasaki, *J. Am. Chem. Soc.*, 2007, **129**, 5257–5263.
7 F. Li, Z. Sun, H. Jiang, Z. Ma, Q. Wang and F. Qu, *Energy Fuels*, 2020, **34**, 11628–11636.
8 J. Zhang, L. Jin, P. Gu, L. Hu, D. Chen, J. He, Q. Xu and J. Lu, *ACS Appl. Nano Mater.*, 2021, **4**, 12407–12414.
9 Z. Li, M. Shao, H. An, Z. Wang, S. Xu, M. Wei, D. G. Evans and X. Duan, *Chem. Sci.*, 2015, **6**, 6624–6631.
10 X. Lu, H. Xue, H. Gong, M. Bai, D. Tang, R. Ma and T. Sasaki, *Nano-Micro Lett.*, 2020, **12**, 86.
11 X. Deng, J. Huang, H. Wan, F. Chen, Y. Lin, X. Xu, R. Ma and T. Sasaki, *J. Energy Chem.*, 2019, **32**, 93–104.
12 X. Zhang, F. Yan, X. Ma, C. Zhu, Y. Wang, Y. Xie, S.-L. Chou, Y. Huang and Y. Chen, *Adv. Energy Mater.*, 2021, **11**, 2102141.

Finite-Element Simulations

Finite-element simulations were performed using the COMSOL Multiphysics commercial package, version 6.1. Three-dimensional models were constructed to simulate SECM experiments in both the negative feedback and SG/TC modes. The “Transport of Diluted Species” (tds) physics interface was utilized to solve steady-state diffusion problems.

1. Parameters

All parameters known from experimental data are defined, including:

- Dimensions of the probe electrode and nanoneedles,
- Diffusion coefficient and concentration of dissolved O_2 in the electrolyte,
- Tip kinetic rate constant, and
- Flux of O_2 generated at the substrate.

2. Geometry

The SECM system geometry was built, representing the electrode body, the sample, and previously validated simulation space (100 times the tip radius in x, y, z). To minimize computational resources geometry simplifications were applied based on the system's symmetry.

3. Boundary Conditions

The boundary conditions (see details in COMSOL report below) were set in the tds interface.

- For negative feedback mode simulations, a no-flux condition was applied to the entire substrate surface.
- For SG/TC mode simulations, a uniform O_2 flux was assigned to the needle surface.
- For simulations involving active sites, an additional flux was assigned to the active spot area.

4. Mesh

A fine computational mesh was constructed, with increased element density in critical regions such as the Pt nanoelectrode disk and the nanoneedle surface, to ensure accurate simulation outcomes.

5. Study

The "stationary" study type was selected. A parametric sweep was performed to vary key parameters, including:

- Tip-to-substrate separation distances,
- Kinetic rate constants, and
- O_2 fluxes.

These parameters were adjusted to fit experimental approach curves.

6. Simulation results

The simulations produced oxygen concentration profiles and SECM tip currents, calculated via surface integration. These results were used to construct theoretical approach curves and extract O_2 fluxes.

COMSOL report

SECM SG/TC mode for OER

Contents

1. Global Definitions

1.1 PARAMETERS

PARAMETERS 1

Name	Expression	Value	Description
at	145[nm]	1.45E−7 m	radius of electrode
RG	1.1	1.1	glass radius
D	2.4e-9[m*m/s]	2.4E−9 m²/s	diffusion coefficient
cbO2	0.25 [mmol/L]	0.25 mol/m³	concentration of O2
L	20	20	distance
id	4*F_const*D*cbO2*n*at	1.3431E−10 A	diffusion current at tip
n	4	4	number of electrons
id_e	id*1.288583525	1.7307E−10 A	RG correction for 1.1
kt	1.7[cm/s]	0.017 m/s	tip kinetics
f	2[nmol/(cm^2*s)]	2E−5 mol/(m²·s)	flux of O2 from substrate
dis_x	0[um]	0 m	x displacement
an	50 [nm]	5E−8 m	needle radius
ln	8 [um]	8E−6 m	needle length
dis_z	1[um]	1E−6 m	z displacement

Name	Expression	Value	Description
f2	90000[nmol/(cm^2*s)]	0.9 mol/(m²·s)	flux of O2 from substrate

2. Component 1

2.1. DEFINITIONS

Coordinate Systems

Boundary System 1

Coordinate system type	Boundary system
Tag	sys1

COORDINATE NAMES

First	Second	Third
t1	t2	n

2.2. GEOMETRY 1

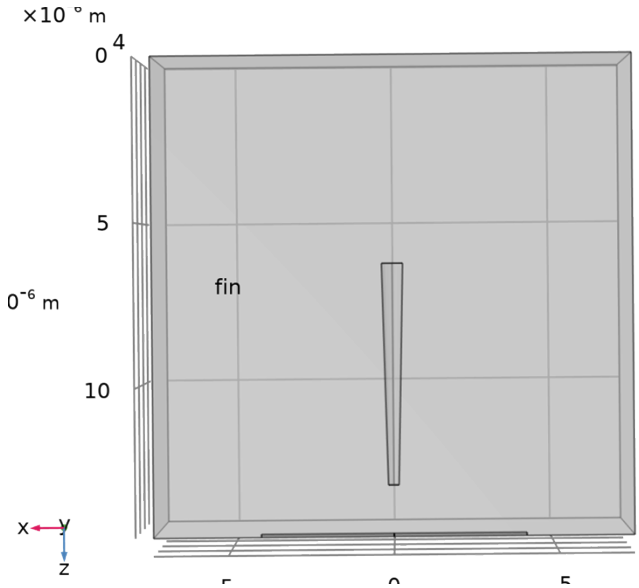

Geometry 1

2.3. TRANSPORT OF DILUTED SPECIES

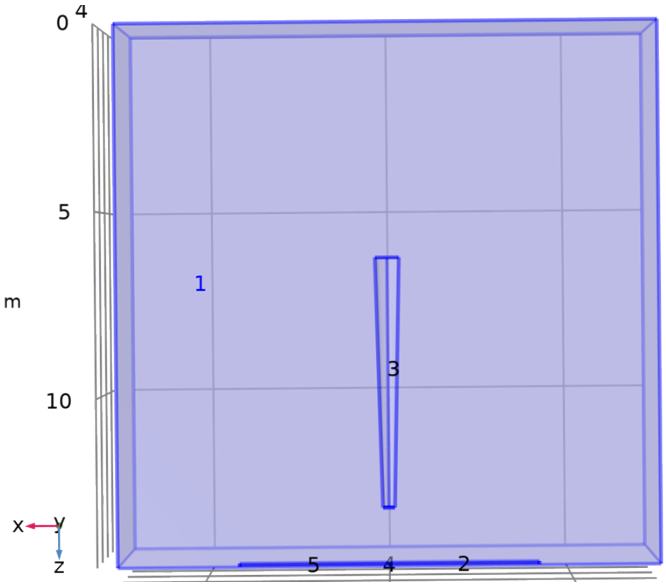

Transport of Diluted Species

EQUATIONS

$$\nabla \cdot \mathbf{J}_i = R_i$$

$$\mathbf{J}_i = -D_i \nabla c_i$$

Transport Properties 1

Transport Properties 1

EQUATIONS

$$\nabla \cdot \mathbf{J}_i = R_i$$

$$\mathbf{J}_i = -D_i \nabla c_i$$

Diffusion

SETTINGS

Description	Value	Unit

Description	Value	Unit
Source	Material	
Material	None	
Diffusion coefficient	User defined	
Diffusion coefficient	D	m²/s

Coordinate System Selection

SETTINGS

Description	Value
Coordinate system	Global coordinate system

Model Input

SETTINGS

Description	Value	Unit
Temperature	User defined	
Temperature	293.15	K

No Flux 1

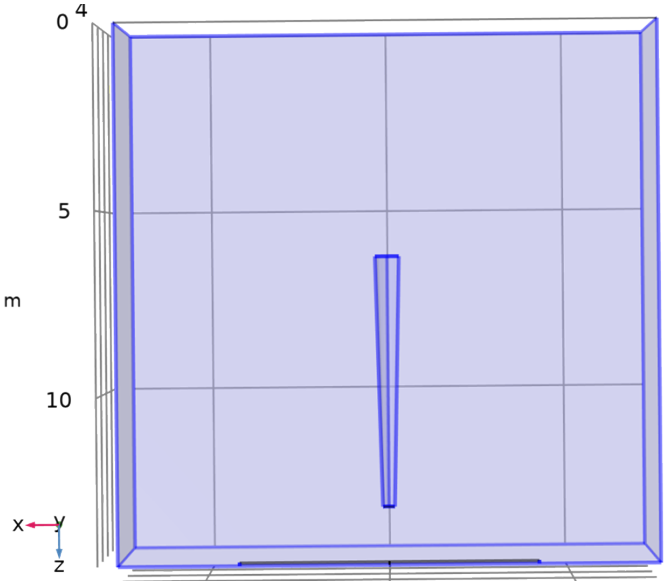

No Flux 1

EQUATIONS

$$-\mathbf{n} \cdot \mathbf{J}_i = 0$$

Initial Values 1

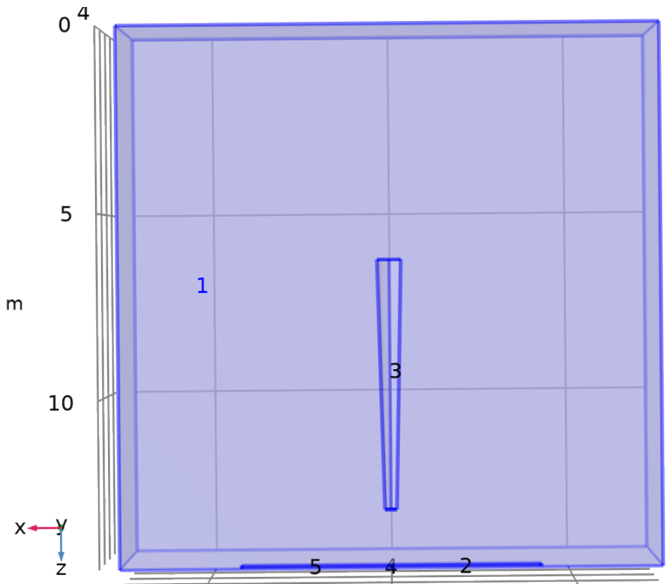

Initial Values 1

Initial Values

SETTINGS

Description	Value	Unit
Concentration	cbO2	mol/m³

bulk concentration on boundaries

bulk concentration on boundaries

EQUATIONS

$$c_i = c_{0,i}$$

Concentration

SETTINGS

Description	Value	Unit
Species cO2	On	
Concentration	cbO2	mol/m³

Flux 1

Flux 1

EQUATIONS

$$-\mathbf{n} \cdot \mathbf{J}_i = \underbrace{J_{0,i}}$$

Inward Flux

SETTINGS

Description	Value	Unit
Flux type	General inward flux	
Species cO2	On	
	f	mol/(m²·s)

Flux 2

Flux 2

EQUATIONS

$$-\mathbf{n} \cdot \mathbf{J}_i = \underbrace{J_{0,i}}$$

Inward Flux

SETTINGS

Description	Value	Unit
Flux type	General inward flux	
Species cO2	On	
	f2	mol/(m²·s)

Symmetry 1

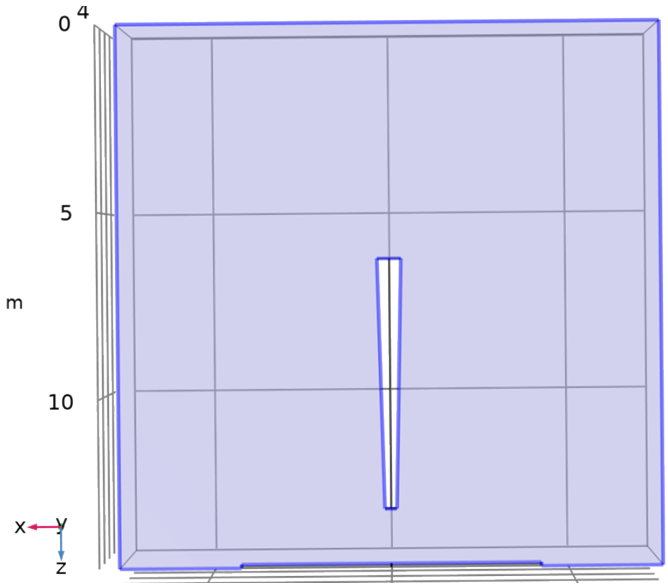

Symmetry 1

EQUATIONS

$$-\mathbf{n}\cdot\mathbf{J}_i = 0$$

Kinetics at the tip

kinetics

EQUATIONS

$$-\mathbf{n}\cdot\mathbf{J}_i = \underset{\cdots}{J_{0,i}}$$

Inward Flux

SETTINGS

Description	Value	Unit
Flux type	General inward flux	
Species cO2	On	
	-kt*cO2	mol/(m²·s)

MESH 1

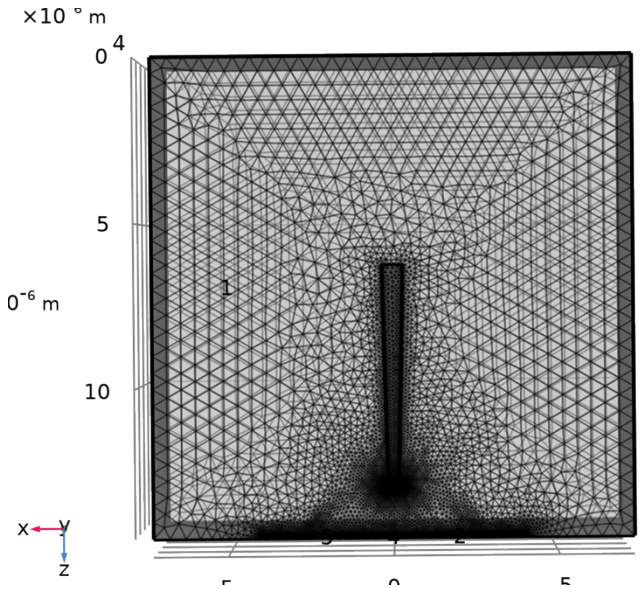

Mesh 1

3. Study 1

3.1. PARAMETRIC SWEEP

Parameter name	Parameter value list

Parameter name	Parameter value list
L	0.05,0.1,0.15,0.2,0.4,0.5,0.8,1,2,3,4,8,10

STUDY SETTINGS

Description	Value
Sweep type	All combinations
Parameter name	L
Unit	

PARAMETERS

Parameter name	Parameter value list	Parameter unit
L (distance)	0.05,0.1,0.15,0.2,0.4,0.5,0.8,1,2,3,4,8,10	

3.2. STATIONARY

STUDY SETTINGS

Description	Value
Include geometric nonlinearity	Off

PHYSICS AND VARIABLES SELECTION

Physics interface	Solve for	Equation form
Transport of Diluted Species (tds)	On	Automatic (Stationary)

MESH SELECTION

Component	Mesh
Component 1	Mesh 1

4. Results

4.1. DERIVED VALUES

Surface Integration 1

OUTPUT

Evaluated in	Table 43

DATA

Description	Value
Dataset	Study 1/Parametric Solutions 1

EXPRESSIONS

Expression	Unit	Description
tds.ntflux_cO2*F_const*n*2	pA	

INTEGRATION SETTINGS

Description	Value
Integration order	4

4.2. PLOT GROUPS

Concentration, Streamline (tds)

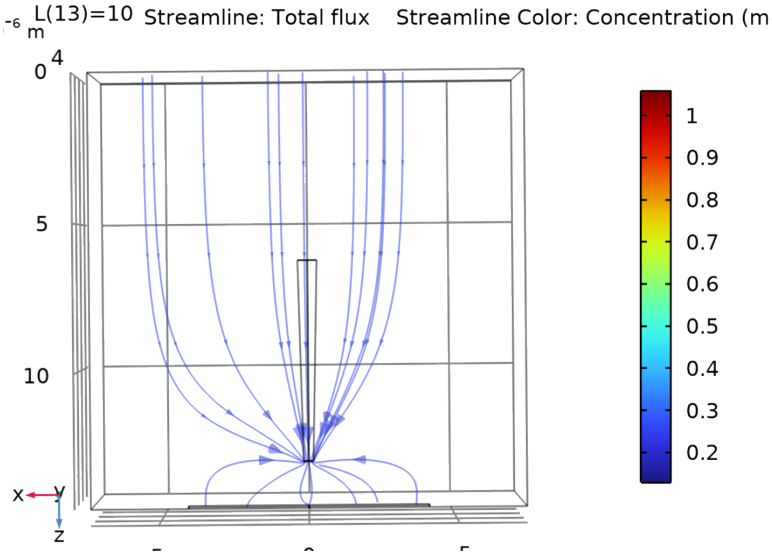

Streamline: Total flux *Streamline Color: Concentration (mol/m³)*

Concentration, Surface (tds)

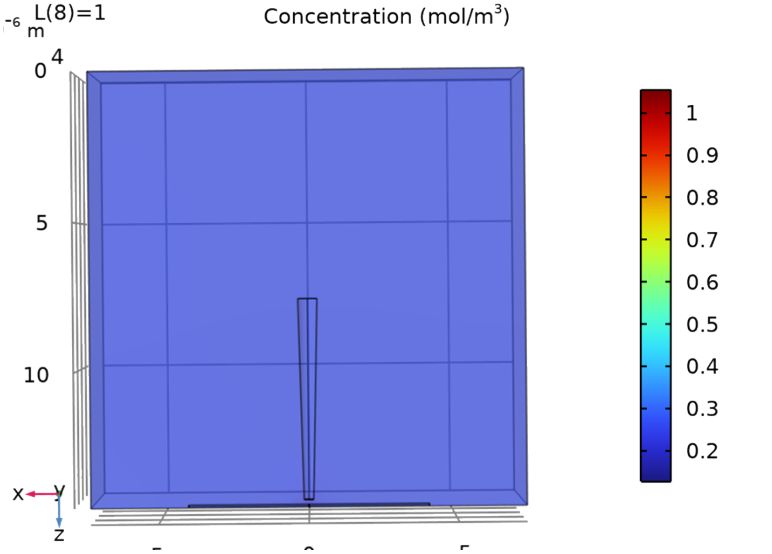

Concentration (mol/m³)

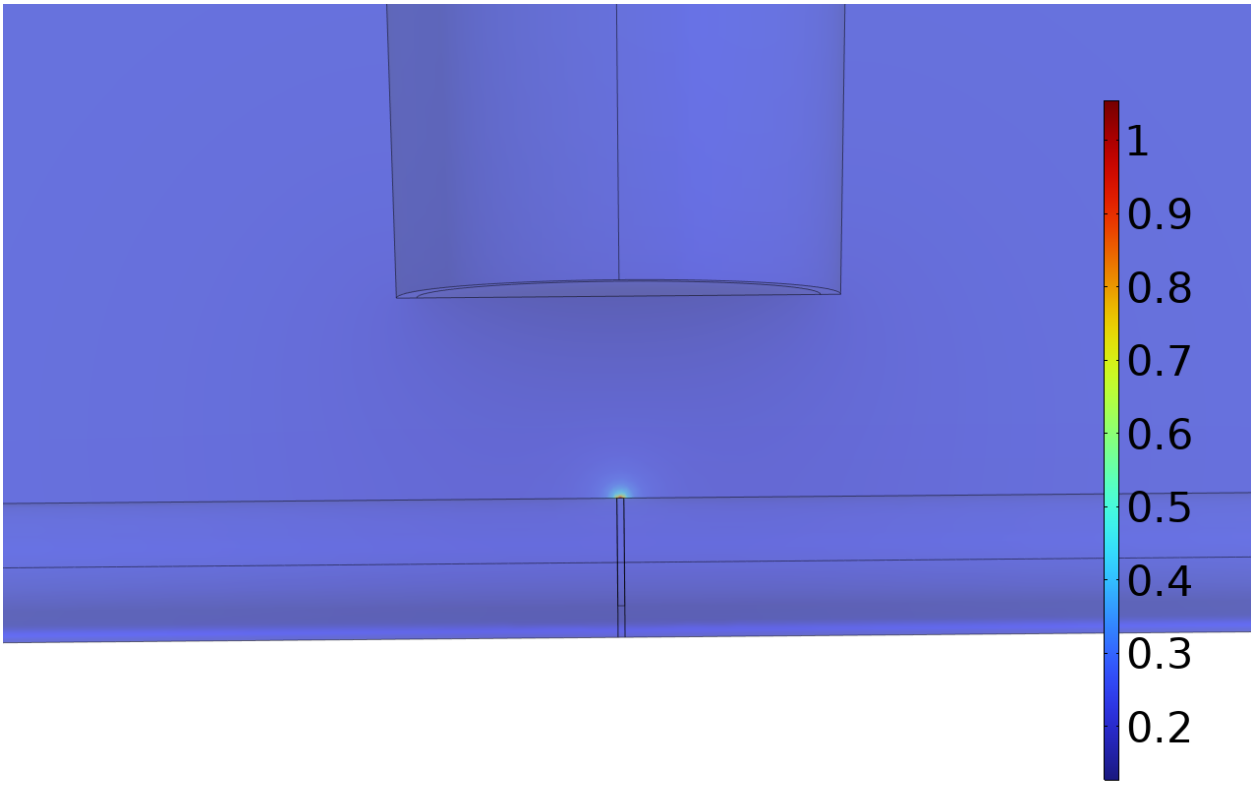
1
0.9
0.8
0.7
0.6
0.5
0.4
0.3
0.2

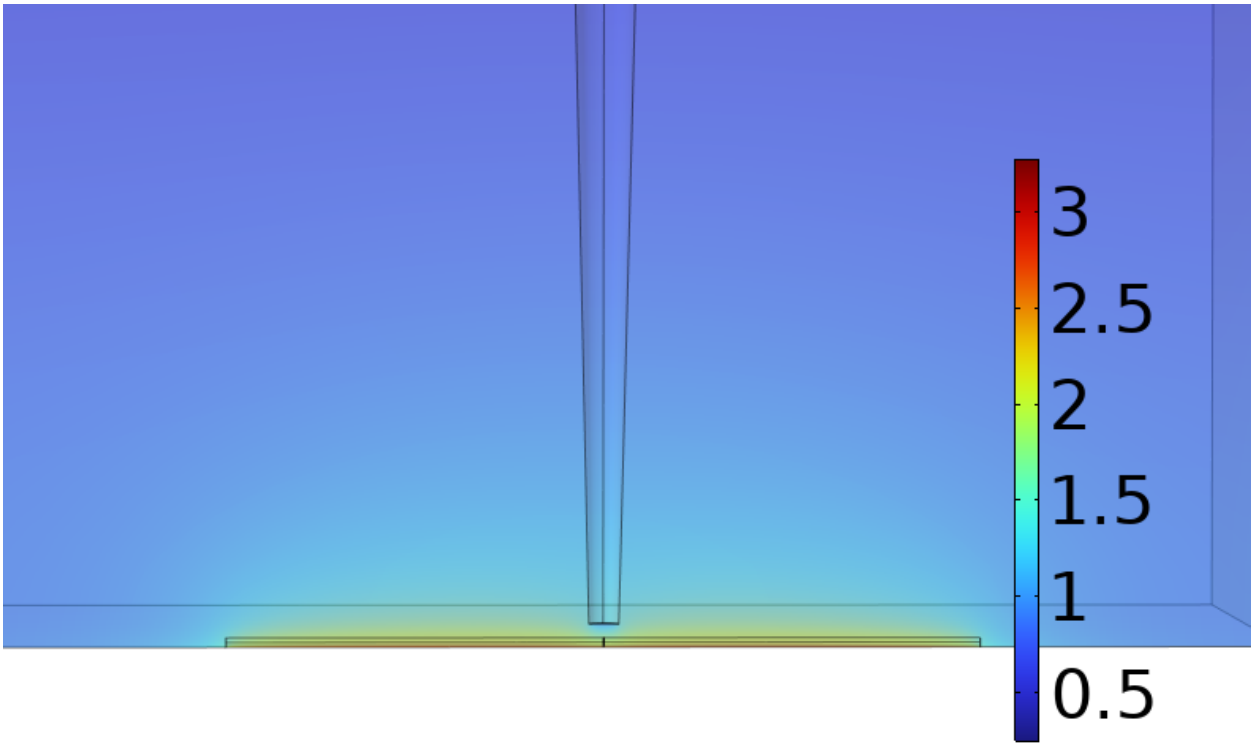
3
2.5
2
1.5
1
0.5